A simple analytical model of complex wall in multibody dissipative particle dynamics

A. Mishra [a,1], A. Hemeda [a,b,1], M. Torabi [a], J. Palko [a], S. Goyal [a], D. Li [a], Y. Ma [a,*]

[a] *School of Engineering, University of California, Merced, CA 95343, United States of America*
[b] *Aerospace Engineering Department, Cairo University, 12613, Egypt*

A R T I C L E   I N F O

A B S T R A C T

In the context of multibody dissipative particle dynamics (MDPD), a closed-form mathematical expression is developed to analytically model a complex wall. MDPD is a modified version of dissipative particle dynamics (DPD), a particle-based mesh free method. There have been several attempts to analytically model the influence of solid walls and non-periodic boundary conditions in the DPD approach. However, there is a limited number of studies for these boundary conditions associated with MDPD that capture static and dynamic fluid-structure interactions through direct modeling of fluid-solid particle interactions. This work, for the first time, employs an analytical model (integral approach) for the solid wall boundary condition in MDPD that brings substantial gain in computational efficiency and thus expands the scope of its applicability to curved or complex walls. Furthermore, a modified model of conservative force is used in the current investigation. The model is first normalized to address the discrepancies in wetting that exist in the present literature and is then validated through several benchmark studies and test cases, such as a Wenzel model. Moreover, comparisons between both the fully numerical and the semi-analytical (integral force model) approaches are drawn. Time efficiency, accuracy, density fluctuation in vicinity of solid wall, and limitations of the proposed model are thoroughly discussed.

© 2019 Elsevier Inc. All rights reserved.

1. Introduction

Wetting is an important phenomenon in various applications such as surfactants, spray cooling and nanolithography [1, 2]. Proper description of wetting is essential to many important problems in the modeling of fluid behavior. Droplet contact angle on a surface is a quantitative metric of surface wettability. There are numerous experimental studies measuring liquid contact angles on surfaces of varying chemistry and geometrical complexity [3–8]. Robust computational approaches to deal with fluid-structure interaction for various droplet sizes and morphological characteristics of the solid surfaces are vital [9,10].

Molecular dynamics and Monte Carlo simulations have been used to study the behavior of droplets on solid surfaces [11–14]. While atomistic methods are very accurate when good interaction potentials are available, these methods are only feasible at the scale about ten nanometers [14–16]. Here, a course-grained method is required to reduce the computational

---

* Corresponding author.
   E-mail address: yma5@ucmerced.edu (Y. Ma).
[1] Equal contribution.

cost at larger scales. There are many different coarse-grained methods which have been used to simulate mesoscale phenomena [17]. Dissipative particle dynamics (DPD) is a particle-based coarse-grained method proposed by Hoogerbrugge et al. [18]. In this approach, each DPD particle (bead) is a cluster of several molecules of a specific fluid/solid/vapor phase (analogous to course-grained modeling in molecular dynamics but with additional particle interactions beyond the conservative terms generally applied in MD) [19]. Later, DPD was applied to simulate hydrodynamic behavior of fluid flow [20]. The main advantage of the DPD approach is in its applicability to the mesoscale regime, which lies between the atomistic and continuum scales [21].

Multibody dissipative particle dynamics (MDPD) is a modified version of DPD which is capable of modeling fluid/fluid and fluid/solid interfaces [22]. For example, MDPD has been used to simulate the classic problem of a sessile droplet [23]. The simulation time scale of MDPD is one to three orders of magnitude larger than conventional molecular dynamics [24]. So far, using DPD and MDPD, several interesting fluid/solid phenomena such as liquid drainage/imbibition from a tube [25], droplet detachment from an AFM tip [26], and several other complex fluid/structure interaction cases [21,27,28] have been investigated. However, in all of the previous studies, dealing with boundary conditions has been a challenging issue [29]. In addition to the fundamental challenges of formulating the wall interactions, common solutions, such as incorporating forces of frozen wall beads, add a drastic computational cost to the modeling. Since the wall particles are frozen, an equivalent interaction formulation from the wall can be found without using the explicit wall beads and significant computational expense can then be saved. The goal of present work is twofold: (*a*) to obtain a consistent set of fluid-solid interaction parameters for a wall consisting of explicit particles, i.e., normalization, and (*b*) to develop a semi-analytical framework to model the wall without the need for explicit wall particles.

In this work, a modified model for fluid-solid interaction is first discussed which can be used to model the three-phase contact line without local density contribution [23]. The governing equations are then normalized and analytically simplified. The model description, algorithm, fluid-solid interaction form, and normalization of the wall density number for the MDPD method is given in section 2. In section 3, the analytical solid wall model is presented followed by validation case studies in section 4. Computational results for one complex geometry with validation of the Wenzel law are discussed in section 5, and they are followed by conclusions in section 6. A brief derivation of the forces using the integral approach is given in Appendix A.

2. Model/algorithm

In MDPD simulations, the motion of particles (or beads) is governed by Newton's second law:

$$\frac{d\vec{r}_i}{dt} = \vec{v}_i, \tag{1}$$

$$m\frac{d\vec{v}_i}{dt} = \vec{F}_i = \sum_{j\neq i}(\vec{F}_{ij}^C + \vec{F}_{ij}^D + \vec{F}_{ij}^R) + \vec{g}, \tag{2}$$

where $\vec{r}_i$, $\vec{v}_i$ and $\vec{F}_i$ denote the ith bead's position, velocity, and the net force exerted on the bead i, respectively, and t is time. The net force is $\vec{F}_i$ which includes body force $\vec{g}$, conservative force $\vec{F}_{ij}^C$, dissipative force $\vec{F}_{ij}^D$ and random force $\vec{F}_{ij}^R$. The three interparticle components are given by [30]:

$$\vec{F}_{ij}^C = A_{ij}\omega_C(r_{ij}, R_c)\vec{e}_{ij} + B(\overline{\rho}_i + \overline{\rho}_j)\omega_C(r_{ij}, R_d)\vec{e}_{ij}, \tag{3}$$

$$\vec{F}_{ij}^D = -\gamma\omega_D(r_{ij}, R_c)(\vec{e}_{ij}.\vec{v}_{ij})\vec{e}_{ij}, \tag{4}$$

$$\vec{F}_{ij}^R = \varphi\omega_R(r_{ij}, R_c)\theta_{ij}\Delta t^{-1/2}\vec{e}_{ij}. \tag{5}$$

Here, in the expression for the conservative force, $\vec{r}_{ij} = \vec{r}_i - \vec{r}_j$ is the position vector from the ith bead to the jth bead with absolute distance of $r_{ij} = |\vec{r}_{ij}|$ and unit vector $\vec{e}_{ij} = \vec{r}_{ij}/|\vec{r}_{ij}|$. Further, A_{ij} and B are the attractive and repulsion force amplitudes, respectively, along with a weighting function of ω_C with two distinct cut-off radii R_c and $R_d = 0.75R_c$, where $\omega_C(r_{ij}, R_c) = \max(1 - r_{ij}/R_c, 0)$. Note that Warren [19] proposed the density-dependent repulsion in the conservative force formula empirically, with the new cut-off range R_d and the local density-function given as [19]

$$\overline{\rho}_i = \frac{15}{2\pi R_d^3}\sum_{j\neq i}\left(1 - \frac{r_{ij}}{R_d}\right). \tag{6}$$

This model has been used in almost all prior works to model both fluid-fluid and fluid-solid interactions. In the present work however, Eq. (3) will not be used in the fluid-solid interaction as will be discussed later in section 2.2.

In the expression for the dissipative force, $\vec{v}_{ij} = \vec{v}_i - \vec{v}_j$ is the velocity of the ith bead relative to the jth bead. The scalars γ and φ are the amplitudes of dissipative and random forces, respectively, and the fluctuation-dissipation theorem [20] requires $\omega_R(r_{ij}, R_c) = \sqrt{\omega_D(r_{ij}, R_c)} = \max(1 - r_{ij}/R_c, 0)$ and $\varphi^2 = 2\gamma k_B T$ where k_B is Boltzmann constant and T is the absolute temperature of the system. The parameter θ_{ij} is Gaussian white noise with unit bandwidth, and Δt is the time step.

Table 1
Parametric values for MDPD simulations.

Parameters	Symbol	MDPD unit
Time step	δt	0.01
Particle mass	m	1.0
Cut-off distance	R_c	1.0
Repulsive interaction range	R_d	0.75
Amplitude of $\vec{F}^D$	γ	5.61
Amplitude of $\vec{F}^{C,A}$	A_{ij}	-40
Amplitude of $\vec{F}^{C,B}$	B	25
System energy	$k_B T$	1.0

2.1. Fluid modeling

In MDPD, reduced units are commonly used for all quantities. The particle mass, cut-off radius R_c and system energy are set to be one in MDPD units. The parameters in Eqs. (1)–(6) for the current modeling approach are listed in Table 1 in MDPD units. One of the many advantages of the MDPD (or DPD) method is that it is a scale-free simulation technique which means one can choose any set of reference parameters, and the results would still hold unchanged. In the present study, the fluid has no viscous effect because it is quasi-static (low capillary number) [26,31]. The reference length is chosen as $L_{DPD} = 1$ μm. By assuming the fluid density and surface tension in the DPD units to be d and σ, respectively, the conversion of mass and time from DPD units to physical ones are [32]

$$M_{DPD} = \frac{d^*}{d} L_{DPD}^3 \tag{7}$$

$$T_{DPD} = \sqrt{M_{DPD} \frac{\sigma}{\sigma^*}} \tag{8}$$

where d^* and σ^* are the physical density and surface tension of the fluid in real units (e.g., SI units) [32]. From the parametric values provided in Table 1, the fluid properties can be calculated. The fluid density, kinematic viscosity and surface tension are calculated as $d = 6.0$, $\vartheta = 7.45$ and $\sigma = 7.31$, respectively, in DPD units. For water as the fluid, the reference scales are found to be $T_{DPD} = 1.29 \times 10^{-7}$ s, and $M_{DPD} = 1.667 \times 10^{-16}$ kg. These scales are conversion factors from the DPD unit system to the physical SI unit system.

2.2. Fluid-solid interaction

Behavior of fluid is the main focus of DPD or MDPD simulations. Thus, particles representing elements of a solid structure such as a wall are generally assumed to be frozen for simplicity [23,33–35]. The fluid-structure interaction is described by the conservative force parameter A_{ij} or A_{sl}, where the subscripts "s" and "l" stand for solid and liquid phases, respectively. The repulsive parameter B is assumed to be constant (same as fluid-fluid interaction) while the attractive parameter A_{sl} is assumed to vary depending on the wall wettability [24,33,36]. The rest of the interaction parameters and/or properties for the solid-liquid particles remain the same as the fluid-fluid ones (see Table 1).

In prior studies using MDPD, the repulsive component of conservative force (Eq. (3)) was defined as a function of local density [22]. Local density is measured based on the number of particles, either of the same type (single-type or liquid) or multi-type particles (i.e., liquid and solid), within the cut-off radius R_d of a given particle. In single-type local density calculations, when the water particle approaches the wall, there is a gradual decrease in the local density for both fluid and wall particles due to the reduction in the number of same type particles within each particles cutoff radius (see Eq. (6)) [23, 24]. In this study, multi-type particle-particle interactions have been used. Recently, the repulsive term in the conservative force has been redefined independent of local density, i.e., a new form of conservative force is used [23]:

$$\vec{F}_{ij}^C = A_{ij}\omega_C(r_{ij}, R_c)\vec{e}_{ij} + B\omega_C(r_{ij}, R_d)\vec{e}_{ij} \tag{9}$$

Using the above expression simplifies the conservative force because there is no local density of the wall in the expression as in conventional MDPD models (see for instance Eq. (3)) [24].

In MDPD simulations using a solid wall, a bounce back scheme (see Fig. 1) is used at the solid boundary which satisfies the no-slip condition at the wall [24]. In the bounce back scheme, the particle returns to its original path if it crosses the solid boundary. The particle travels the same distance along this path as it would have traveled if the boundary had not been present. As shown in Fig. 1, the velocity and force in the bounce-back scheme reverse their directions [37].

2.3. Normalization

In previous studies [22–24,28,32,38,39], the results from the simulation of a droplet on a wall depend on the density of wall particles, which is unphysical when representing a solid wall. To have the results independent of wall density, a
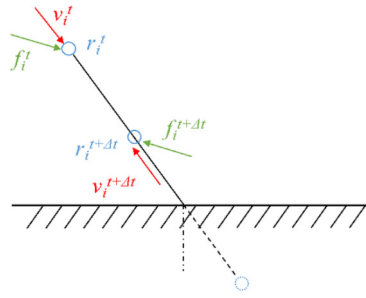
Fig. 1. Representation of bounce-back scheme.

Table 2
Wall density number ρ_s used in prior work and the range of corresponding A_{sl}.

ρ_s	$-A_{sl}$ (or A) range	Method	Local density approach	Reference
6.0	–	MDPD	Multi-type	[22]
8.0	15–40	MDPD	Multi-type	[38]
4.0–8.0	8–23	DPD	–	[28]
6.88	5–40	MDPD	Multi-type	[39]
25	6–12	MDPD	Single-type	[23]
5.12	25–50	MDPD	Multi-type	[32]
6.0	8–22	MDPD	Single-type	[24]

normalization of the local density is needed. In prior work, many choices for the number density of the wall have been tried resulting in inconsistent A_{sl}. In several studies, the wall density is taken to be equal to the fluid density [21] while in some other studies the wall number density is significantly higher than the fluid density [23].

In Table 2, wall density from some studies is shown. As can be seen from Table 2, because of different number densities and/or local density approaches, different A_{sl} values or ranges have been obtained in these studies. The large A_{sl} range is a result of variation in liquid and wall density at the interfaces. In other words, when the number density of the wall changes, the magnitude of the force on fluid particle varies, and thus, the interaction between wall and fluid particle differs. Hence, there has not been any consistent scale for A_{sl} for different wettability of a surface. Figure 2a shows the effect of A_{sl} on the contact angle of a water droplet on a flat wall for different number densities of the solid wall particles. To calculate the contact angle, the boundary of the droplet is found by calculating the local density of the particles throughout the droplet (see the inset in Fig. 2a). As can be seen, the change in the A_{sl} range due to the solid wall density number is clear and it is in agreement with prior work in Table 2. This can be explained from Eq. (3) where increasing solid wall particle density increases the repulsion force. Hence, smaller attraction force (in absolute value) is needed to obtain the same contact angle. It is concluded that lower values of A_{sl} result in the same contact angle for a wall with a higher density.

Contact angle of a droplet also changes with the number of fluid particles it contains [40]. In this study, the fluid particle number is assigned to be around 13,000 and kept the same throughout the study. To obtain consistent results independent of the wall density, the solid wall particles' contribution in both local density and forces calculations are normalized. For example, the modified liquid local density $\overline{\rho}^*$ can be written as $\overline{\rho}^* = \frac{\rho_l}{\rho_s}\overline{\rho}$ where ρ_l and ρ_s are number densities of liquid and solid, respectively. We therefore split the summation in the local density of the liquid particle into liquid neighbors' contribution (l) and solid neighbors' contribution (s) as shown in Eq. (10)

$$\overline{\rho}_i = \frac{15}{2\pi R_d^3}\left[\sum_{j\neq i}^{l}\left(1 - \frac{r_{ij}}{R_d}\right)^2 + \frac{\rho_l}{\rho_s}\sum_{j\neq i}^{s}\left(1 - \frac{r_{ij}}{R_d}\right)^2\right] \tag{10}$$

Note that for simplicity the subscript "i" for the ith particle is dropped in the rest of the work, e.g., $\overline{\rho} = \overline{\rho}_i$ or $F = F_i$ due to wall. In Eq. (10), the second term in the right-hand side (summation over solid neighbors) is scaled with the density ratio of liquid and solid. In other words, the contribution of the solid wall particles in either the local density or the force calculations will be normalized as given in Eq. (10) for any given value of ρ_s.

Figure 2b depicts the change in the contact angle of a water droplet of a flat wall after normalization. As expected, the contact angle for each A_{sl} number asymptotically approaches a constant value at higher solid wall density number. Although such an approach has been already proposed in DPD modeling [28,35], we apply it to MDPD simulations for the first time in the present investigation. Analytical expressions derived for solid wall interaction forces on adjoining fluid particles are discussed in the following section.
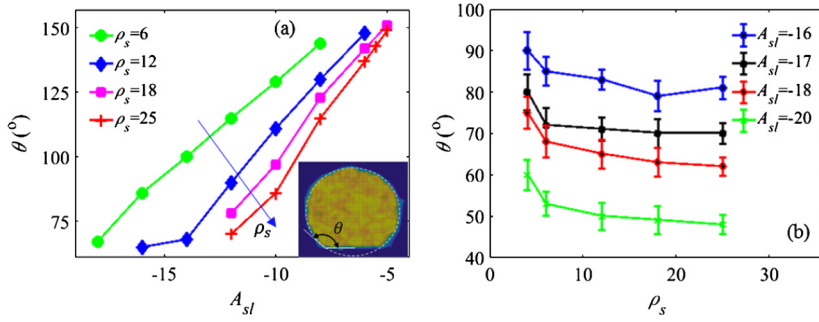
Fig. 2. Effect of A_{sl} on the droplet contact angle θ on a flat surface with different solid wall density number ρ_s in (a). After normalization, the effect of solid wall number density ρ_s on the droplet contact angle θ for different A_{sl} in (b). The inset figure shows the local density distribution contour used to predict the contact angle using spherical cap approach in (a). (For interpretation of the references to color in this figure, the reader is referred to the web version of this article.)
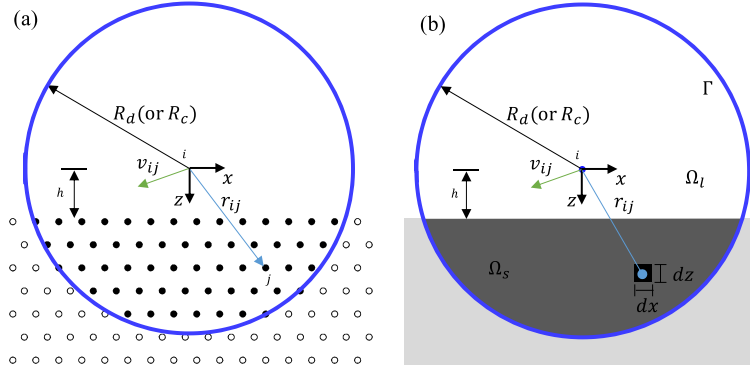

Fig. 3. Schematic for the portion of wall particles within a cutoff radius R_d (or R_c) that contributes to the force on liquid particle i for particle-particle approach (black shaded particle) in (a) and integral approach (dark-gray area) in (b).

3. Integral approach for wall boundary

While the wall particles are frozen, these particles still take part in the calculation for the fluid particles as neighbors. More specifically, the fluid particles that are closer to the wall have wall particles within their cut-off radius, and there is a component of force due to these wall particles. This study focuses on imposing a force due to a wall via applying an analytical formulation, rather than considering each pairwise interaction with the frozen wall particles. A set of algebraic expressions (i.e., forces) for the boundary is used to represent the solid wall. This approach significantly reduces the computational cost of simulations, especially for a highly dense wall. The resultant force on an MDPD particle due to the wall is derived by integrating the force due to each individual wall particle. Note that we again split the summation terms into two sets for liquid and for solid neighbors, and an integral approach is then used to find a closed-form expression for the wall particle contribution (see for instance Eq. (10)) [28]. Generally, these formulae or expressions are given by the following equations:

$$\langle Y \rangle = 2\pi \int\limits_{z=h}^{R_d} \int\limits_{r=0}^{\sqrt{R_d^2-z^2}} \left[\rho_l g(r) Y \right] r \, dr \, dz \tag{11}$$

where $g(r)$ is the radial distribution function of the DPD particle, and $\langle Y \rangle$ is the integral value of Y within the cut-off radius R_d (or R_c) on the domain Ω_s [28,35] as shown in Fig. 3a (particle-particle interaction) and 3b (integral approach). Note that the factor 2π represents the axi-symmetry of the domain in the 3D configuration (Fig. 3). The value Y can be either a local density function or force component as will be discussed below. Also, because of the high wall density, the radial distribution function $g(r)$ is assumed to be 1.0 in this work [28].

For the local density due to the solid wall, the Y-term in Eq. (11) is replaced by Eq. (6), then the summation is replaced by the integration. The local density due to the wall at particle i, $\overline{\rho}_{i,s}$, can be expressed as

$$\overline{\rho}_{i,s}(\delta_d) = \rho_l \times \left[0.5 - \frac{5}{4}\delta_d + \frac{5}{2}\delta_d^3 - \frac{5}{2}\delta_d^4 + \frac{3}{4}\delta_d^5 \right] \tag{12}$$
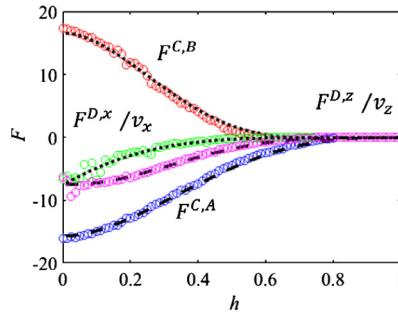
Fig. 4. Comparison of the results between the particle (symbols) and integral (dash and dotted lines) approaches as function of spacing h from the solid wall as shown in Fig. 3, conservative force components and x and z components of the dissipative forces.

where $\delta_d = h/R_d$ (see Fig. 3). This term will be added to the local density for particle i which represents the wall effect in multi-type particle density calculations. In other words, the local density for particle i is now $\bar{\rho}_i = \bar{\rho}_{i,s} + \frac{15}{2\pi R_d^3} \sum_{j \neq i}^{l} (1 - r_{ij}/R_d)^2$ where j is the list of the DPD liquid neighbors to the particle i within the cut-off radius R_d.

For the conservative force, Eq. (9) will be integrated in the domain Ω_s. Due to the axisymmetric design of the geometry, there will be only a z-component of the conservative force (i.e., forces in the x–y plane vanish, see Fig. 3b). The attractive force in the z-direction is here named $F^{C,A}$ which was originally $A_{ij}\omega_c(r_{ij}, R_c)\vec{e}_{ij}$. Using Eq. (11), this force can be reduced to

$$F^{C,A}(\delta) = 2\pi R_c^3 A_{sl} \rho_l \times \left[\frac{1}{24} - \frac{1}{4}\delta^2 + \frac{1}{3}\delta^3 - \frac{1}{8}\delta^4 \right] \tag{13}$$

Again, we choose $\delta = h/R_c$ (see Fig. 3). Note that the conservative repulsive force $F^{C,B}$ has the same form as the attraction force but within a cut-off radius of R_d (δ is replaced with $\delta_d = h/R_d$) and with amplitude of B. For the dissipative force components ($F^{D,x}$ and $F^{D,z}$), the integration is repeated, with

$$F^{D,x}(\delta) = -2\pi \gamma v_x \rho_l \times \left[\frac{1}{45} - \frac{1}{12}\delta + \delta^3 \times \left\{ \frac{2}{9} + \frac{1}{3}\log(\delta) \right\} + \frac{1}{3}\delta^4 - \frac{1}{20}\delta^5 \right] \tag{14}$$

$$F^{D,z}(\delta) = -\pi \gamma v_z \rho_l \times \left[\frac{1}{90} + \delta^3 \times \left\{ \frac{7}{18} + \frac{1}{4}\log(\delta) \right\} - \frac{1}{2}\delta^4 + \frac{1}{10}\delta^5 \right] \tag{15}$$

where v_x and v_z are the velocity components in the x- and z-directions, respectively. The random force vector is expressed as

$$\vec{F}^D(\delta) = F^{D,x}(\delta)\boldsymbol{e_x} + F^{D,z}(\delta)\boldsymbol{e_z} \tag{16}$$

where

$$\vec{F}^R(\delta) = \xi \left[\sqrt{2k_B T F^{D,x}(\delta)}\boldsymbol{e_x} + \sqrt{2k_B T F^{D,z}(\delta)}\boldsymbol{e_z} \right] \tag{17}$$

and ξ is the random variable with Gaussian distribution [35]. The details of these derivations are given in Appendix A.

Now, this set of equations (Eqs. (12)–(16)) can be used to simplify the numerical modeling by removing the solid wall from the calculations. The equations are validated by comparison to the explicit particle approach and forces are compared in Fig. 4. The model is derived for a flat wall; however, it can also be used for curved walls with large radius of curvature as will be shown in section 6. If the radius of curvature of the wall R_{wall} is within a certain limit ($R_{wall} > 3R_c$), the model is valid and can be used with the error being less than 5%, as will be seen in the following sections.

4. Validation

To validate our model, we simulate a droplet on a flat wall, and we generate a similar relationship between contact angle and A_{sl} (see Fig. 5). For this simulation, total number of fluid particles is 13,062 in both integral and particle approaches. In particle approach, the total number of wall particles is 85,312, where the wall density is chosen to be $\rho_s = 25.0$. We compared this relationship with available literature [23], and an excellent agreement is obtained, especially at small A_{sl}. In our analytical approach, the equation is integrated using the value of $\rho_l = 6.0$. With the analytical approach, we save more than 50% of computational cost for this case. More details of computational savings will be discussed in section 5.

In order to evaluate the capabilities and stability of the present model, the density fluctuation in vicinity to solid wall and thermal energy, $k_B T$, are calculated for a droplet on a solid flat wall. The same droplet configuration used in Fig. 5 is considered here with an $A_{sl} = -16$ or $\theta \sim 100°$. For the density fluctuation, rectangular blocks (bins) with dimensions of $10 \times 10 \times 0.1$ are considered in the core of the droplet as shown in the inset in Fig. 6a. The average density number (temporal
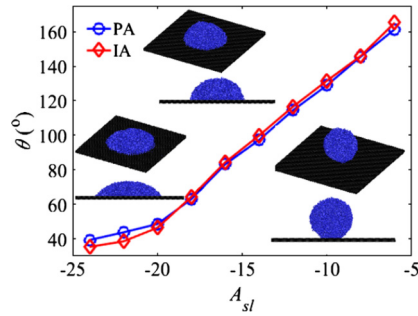
Fig. 5. Comparison between the contact angle using particle-particle and integral approaches for different A_{sl}.
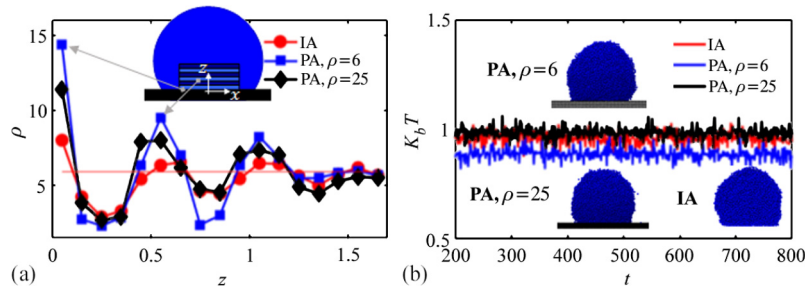

Fig. 6. Comparison between the results from the particle approach (PA) and integral approach (IA) on (a) local density fluctuations, ρ, in vicinity to solid wall, (b) temporal thermal energy, $k_B T$.
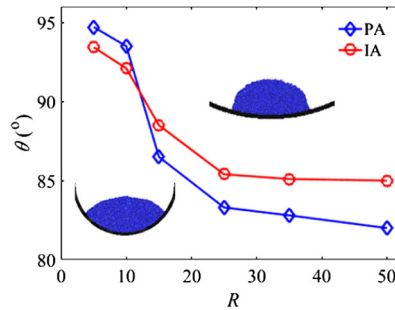

Fig. 7. Effect of surface curvature on contact angle for the particle approach (PA) and integral approach (IA).

and spatial average) is calculated in these bins in the same fashion of molecular dynamic simulations [41–44]. As expected, increasing the wall density number damps the density perturbation near the solid wall as shown in Fig. 6a. Moreover, the results from the integral approach (IA) shows the minimum fluctuations around the average density (about 6.1). $k_B T$ can be calculated form the kinetic energy for the water droplet, i.e., $\frac{3}{2} k_B T = \frac{m}{2N} \sum_i \vec{v}_i . \vec{v}_i$ where N is the number of DPD particles in the water droplet. This specific energy, $k_B T$, is shown in Fig. 6b for different wall density numbers for particle approach (PA) and integral approach (IA). The results show an excellent agreement with the isothermal approximation of the MDPD modeling of this system (see for instance Table 1).

Further, we use the IA to simulate a droplet on a curved surface and compare it with the PA. Contact angle on a droplet for a curved surface can no longer be defined using Young's equation [45], i.e., the contact angle in this case is not the same as the one on a flat plate. For a hydrophilic droplet, the contact angle on a curved surface is higher than the contact angle for a droplet on a flat plate. By varying the radius of the curved surface to infinity, it ultimately corresponds to a flat plate and the contact angle of the droplet converges to its contact angle of flat plate. In Fig. 7, the contact angle of a droplet for one hydrophilic case is shown for various radii of curvature and the contact angle is different for different radii. The contact angle is found to reach a constant value after reaching a certain radius of curvature, asymptotically converging to its value on the flat surface.
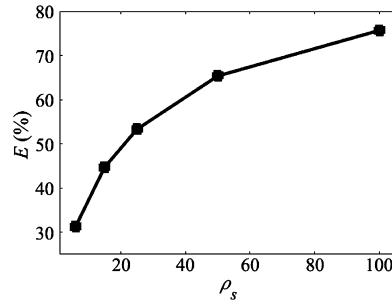
Fig. 8. The percentage reduction in the CPU time E using the integral approach against its counterpart particle approach.
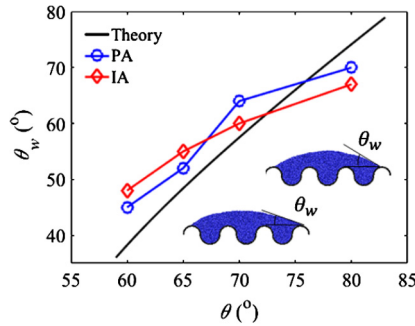

Fig. 9. The comparison of analytical results with theoretical equation for Wenzel law.

5. Results and discussion

The analytical model was validated and compared with the explicit all particle simulations in section 4. For the comparison, a wall number density of 25 has been taken in particle simulations. In this section, the advantage and limitations of the integral approach are given.

The CPU time reduction is expressed using the percentage $E(\%)$ as

$$E(\%) = \frac{t_{PA} - t_{IA}}{t_{PA}} \times 100 \tag{18}$$

where t is the CPU time used in the simulation, and the subscripts "PA" and "IA" stand for the particle-particle and integral approaches, respectively.

The time consumed to obtain the results shown in Fig. 5 is used to calculate E with different solid wall density numbers as shown in Fig. 8. As the wall density number increases, the number of wall particles participating in the computational algorithm also increases. On the other hand, in the integral approach, the total number of particles remains the same (liquid particle), thus computational cost remains almost unchanged. Moreover, with increasing complexity in geometry, wall density and domain size, the particle-particle approach tends to have more computational cost when compared to the integral model. In the integral approach, the computational cost primarily depends on liquid particle numbers, thus when the wall complexity is increased, the integral approach is clearly the more efficient between the two approaches.

To describe the homogeneous wetting regime, the Wenzel model has been previously used [46]. According to the Wenzel model, the contact angle on a rough surface can be estimated by

$$\cos\theta_W = r\cos\theta \tag{19}$$

where θ_W is the Wenzel angle, r is surface roughness ratio and θ is the contact angel on a flat surface. Roughness ratio is defined as

$$r = \frac{A_s}{A_{s0}} \tag{20}$$

where A_s is area of the surface, and A_{s0} is the projected area of the surface. A 2D geometry is taken into consideration to validate the analytical approach for a complex wall geometry (see Fig. 9).

In Fig. 9, results from Wenzel equation validations are shown. Contact angle is depicted against Wenzel contact angle for theoretical, numerical and semi-analytical counterparts. The analytical approach shows good agreement with both the particle approach and theoretical approaches. This is also an extra validation of the model used in the present work. Finally, a substantial amount of computational time has been saved in such geometries (about 45%) with $\rho_s = 25$. This is because of the highly curved wall, which adds a substantial number of extra particles compared to the flat wall.

6. Conclusions

In previous MDPD works, different wall densities had been used, which resulted in different ranges of A_{sl} values (solid-liquid interaction parameter) for wetting characterization. To solve this discrepancy in the literature, normalization is first carried out in this work. A consistent A_{sl} range is obtained for different surface wettability. To do so, a high wall number density number (e.g. 25 or more) is required. The particle approach (PA) used in previous works for the wall is computationally expensive for large domains, high wall density, and complex geometry. In this work, a wall model is developed using a combination of analytical and numerical integration, which substantially reduces the computational cost. As the wall complexity and domain size are increased, it is shown that this model has an advantage over traditional particle approaches. The conventional particle approach for the wall takes about 100–300% more time when compared to the presented integral model for the same geometrical configuration. The results for the test cases are compared with those obtained from the particle approach and they match well. Thus, the analytical wall model provided in this investigation is an accurate and simple tool to simulate fluid-structure interaction in MDPD while saving computational time. In addition, compared with the particle approach, there is remarkable reduction in density fluctuation in vicinity of solid wall for the integral approach. The presented integral (derived for a flat wall) also gives accurate results for walls with sufficiently large curvature. The minimum radius of curvature to which it can be applied accurately is $\sim 3R_c$. This limitation of the model needs to be addressed in future work.

Acknowledgement

Appendix A. Numerical and analytical integration of wall forces

In this work, the forces due to the solid wall are derived using a combination of numerical and analytical expressions. These equivalent forces have been used for all the simulation procedures. In the particle-particle approach, the wall is made of particles (see Fig. 2a), which means for a fluid particle i, individual pair-wise forces resulting from each wall particle are calculated using the Eqs. (4), (5) and (9). The resultant force on the fluid particle due to the wall is the sum of the forces by each individual wall particle within the cut-off radius. As the number density increases, the number of particles in the zone within the cut-off radius for the particle i increases. Force on the fluid particle due to one wall particle is governed by [23]

$$\vec{F}_{ij}^C = A_{ij}\omega_C(r_{ij}, R_c)\vec{e}_{ij} + B\omega_C(r_{ij}, R_d)\vec{e}_{ij} \tag{21}$$

Total conservative force on particle i due to the full wall is governed by

$$\vec{F}^{C,A} = \sum_{j \neq i} \vec{F}_{ij}^C = \sum_{j \neq i} \left(A_{ij}\omega_C(r_{ij}, R_c)\vec{e}_{ij} + B\omega_C(r_{ij}, R_d)\vec{e}_{ij} \right) \tag{22}$$

Ideally, the actual number density of 25.0 or more is enough to make the wall essentially continuous. This wall density is normalized for the wall number density (i.e., $\rho_l = 6.0$) as explained in section 2. For a continuous wall, the summation changes to integration. For instance, if we express any term due to wall in the conservative attractive force term (Eq. (9)) in the integration form then it will become

$$F^{C,A} = \int_{z=h}^{R_c} \int_{x=0}^{\sqrt{R_c^2-z^2}} \int_{\theta=0}^{2\pi} \rho_l \left(A_{ij}\omega_C(r_{ij}, R_C)\vec{e}_{ij} \right) x\, dx\, d\theta\, dz \tag{23}$$

where $F^{C,A}$ is attractive component of the conservative force. It can further be simplified and expressed as

$$F^{C,A} = 2\pi\rho_l A_{ij} \int_{z=h}^{R_c} \int_{x=0}^{\sqrt{R_c^2-z^2}} \left(\left(1 - \frac{r}{R_c}\right)\vec{e}_{ij} \right) x\, dx\, dz \tag{24}$$

where $r^2 = x^2 + z^2$. Upon integration, Eq. (13) is obtained (Eq. (25)):

$$F^{C,A} = 2\pi R_c^3 A_{sl}\rho_l \times \left[\frac{1}{24} - \frac{1}{4}\delta^2 + \frac{1}{3}\delta^3 - \frac{1}{8}\delta^4 \right] \tag{25}$$

where $\delta = h/R_c$. As discussed before, the conservative attraction force has identical form but with cut-off radius R_d and amplitude B. Similarly, integrations are performed for the dissipative and random components of force, and the following expressions are derived

$$F^{D,x}(\delta) = -2\pi\,\gamma\,v_x\rho_l \times \left[\frac{1}{45} - \frac{1}{12}\delta + \delta^3 \times \left\{\frac{2}{9} + \frac{1}{3}\log(\delta)\right\} + \frac{1}{3}\delta^4 - \frac{1}{20}\delta^5\right] \tag{26}$$

$$F^{D,z}(\delta) = -\pi\,\gamma\,v_z\rho_l \times \left[\frac{1}{90} + \delta^3 \times \left\{\frac{7}{18} + \frac{1}{4}\log(\delta)\right\} - \frac{1}{2}\delta^4 + \frac{1}{10}\delta^5\right] \tag{27}$$

$$\vec{F}^R = \xi\left[\sqrt{2k_BTF^{D,x}(\delta)}\,\boldsymbol{e_x} + \sqrt{2k_BTF^{D,z}(\delta)}\,\boldsymbol{e_z}\right] \tag{28}$$

where v_x and v_z are the particle's velocity in the x and z directions (see Section 3).

References

[1] D. Bonn, J. Eggers, J. Indekeu, J. Meunier, Wetting and spreading, Rev. Mod. Phys. 81 (2009) 739–805, https://doi.org/10.1103/RevModPhys.81.739.
[2] A. Marmur, Wetting on real surfaces, J. Imaging Sci. Technol. 44 (2000) 406–409.
[3] R.N. Wenzel, Surface roughness and contact angle, J. Psychosom. Res. 53 (1949) 1466–1467, https://doi.org/10.1016/0022-3999(86)90018-8.
[4] H. Kusumaatmaja, J.M. Yeomans, Modeling contact angle hysteresis on chemically patterned and superhydrophobic surfaces, Langmuir 23 (11) (2007) 6019–6032, https://doi.org/10.1021/la063218t.
[5] M.M. Amrei, M. Davoudi, G.G. Chase, H.V. Tafreshi, Effects of roughness on droplet apparent contact angles on a fiber, Sep. Purif. Technol. 180 (2017) 107–113, https://doi.org/10.1016/j.seppur.2017.02.049.
[6] D.G. Venkateshan, H.V. Tafreshi, Modelling droplet sliding angle on hydrophobic wire screens, Colloids Surf. A 538 (2018) 310–319, https://doi.org/10.1016/j.colsurfa.2017.11.003.
[7] M. Abolghasemibizaki, R.L. McMasters, R. Mohammadi, Towards the shortest possible contact time: droplet impact on cylindrical superhydrophobic surfaces structured with macro-scale features, J. Colloid Interface Sci. 521 (2018) 17–23, https://doi.org/10.1016/j.jcis.2018.03.005.
[8] M. Abolghasemibizaki, C.J. Robertson, C.P. Fergusson, R.L. McMasters, R. Mohammadi, Rolling viscous drops on a non-wettable surface containing both micro- and macro-scale roughness, Phys. Fluids 30 (2018), https://doi.org/10.1063/1.5016824.
[9] G. Hou, J. Wang, A. Layton, Numerical methods for fluid-structure interaction – a review, Commun. Comput. Phys. 12 (2018) 337–377, https://doi.org/10.4208/cicp.291210.290411s.
[10] P. Meakin, Dissipative particle dynamics and other particle methods for multiphase fluid flow in fractured and porous media, Prog. Comput. Fluid Dyn., Int. J (2008), https://doi.org/10.1504/PCFD.2009.027371.
[11] A.V. Lukyanov, A.E. Likhtman, Dynamic contact angle at the nanoscale: a unified view, ACS Nano (2016), https://doi.org/10.1021/acsnano.6b01630.
[12] S. Do, M. Yeong, S. Balachandar, Static and dynamic contact angles of water droplet on a solid surface using molecular dynamics simulation, J. Colloid Interface Sci. 339 (2009) 187–195, https://doi.org/10.1016/j.jcis.2009.07.048.
[13] D. Sergi, G. Scocchi, A. Ortona, Molecular dynamics simulations of the contact angle between water droplets and graphite surfaces, Fluid Phase Equilib. 332 (2012) 173–177, https://doi.org/10.1016/j.fluid.2012.07.010.
[14] N. Ojaghlou, H.V. Tafreshi, D. Bratko, A. Luzar, Dynamical insights into the mechanism of a droplet detachment from a fiber, Soft Matter (2018), https://doi.org/10.1039/C8SM01257A.
[15] S. Plimpton, Fast parallel algorithms for short – range molecular dynamics, J. Comput. Phys. 117 (1995) 1–19, https://doi.org/10.1006/jcph.1995.1039.
[16] T.A. Arias, M.C. Payne, J.D. Joannopoulos, Ab initio molecular-dynamics techniques extended to large-length-scale systems, Phys. Rev. B 45 (1992) 1538–1549, https://doi.org/10.1103/PhysRevB.45.1538.
[17] T. Kinjo, S. Hyodo, Linkage between atomistic and mesoscale coarse-grained simulation, Mol. Simul. 33 (2007) 417–420, https://doi.org/10.1080/08927020601155436.
[18] P.J. Hoogerbrugge, J.M.V.A. Koelman, Simulating microscopic phenomena with dissipative particle dynamics, Europhys. Lett. 19 (1992) 155–160.
[19] P.B. Warren, Hydrodynamic bubble coarsening in off-critical vapor-liquid phase separation, Phys. Rev. Lett. 87 (2001) 225702, https://doi.org/10.1103/PhysRevLett.87.225702.
[20] P. Español, P. Warren, Statistical mechanics of dissipative particle dynamics, Europhys. Lett. 30 (1995) 191–196, https://doi.org/10.1209/0295-5075/30/4/001.
[21] R.D. Groot, P.B. Warren, Dissipative particle dynamics: bridging the gap between atomistic and mesoscopic simulation, J. Chem. Phys. 107 (1997) 4423–4435, https://doi.org/10.1063/1.474784.
[22] P.B. Warren, Vapor-liquid coexistence in many-body dissipative particle dynamics, Phys. Rev. E (2003) 1–8, https://doi.org/10.1103/PhysRevE.68.066702.
[23] N. Ghorbani, A. Pishevar, A mesoscopic simulation of static and dynamic wetting using many-body dissipative particle dynamics, Comput. Part. Mech. 5 (2018) 113–123, https://doi.org/10.1007/s40571-017-0157-4.
[24] Z. Li, G. Hu, Z. Wang, Y. Ma, Z. Zhou, Three dimensional flow structures in a moving droplet on substrate: a dissipative particle dynamics study, Phys. Fluids 25 (2013) 072103, https://doi.org/10.1063/1.4812366.
[25] C. Chen, L. Zhuang, X. Li, J. Dong, J. Lu, A many-body dissipative particle dynamics study of forced water-oil displacement in capillary, Langmuir 28 (2012), https://doi.org/10.1021/la204207s.
[26] M. Ahmadlouydarab, A.A. Hemeda, Y. Ma, Six stages of microdroplet detachment from microscale fibers, Langmuir 34 (2018) 198–204, https://doi.org/10.1021/acs.langmuir.7b03089.
[27] C. Lan, S. Pal, Z. Li, Y. Ma, Numerical simulations of the digital microfluidic manipulation of single microparticles, Langmuir 31 (2015) 9636–9645, https://doi.org/10.1021/acs.langmuir.5b02011.
[28] Z. Li, X. Bian, Y. Tang, G. Em, A dissipative particle dynamics method for arbitrarily complex geometries, J. Comput. Phys. 355 (2018) 534–547, https://doi.org/10.1016/j.jcp.2017.11.014.
[29] M. Revenga, I. Zúñiga, P. Español, Boundary conditions in dissipative particle dynamics, Comput. Phys. Commun. 121 (1999) 309–311, https://doi.org/10.1016/S0010-4655(99)00341-0.
[30] A. Boromand, S. Jamali, J.M. Maia, Viscosity measurement techniques in dissipative particle dynamics, Comput. Phys. Commun. 196 (2015) 149–160, https://doi.org/10.1016/j.cpc.2015.05.027.
[31] C. Cupelli, B. Henrich, T. Glatzel, R. Zengerle, M. Moseler, M. Santer, Part. Dyn. 10 (2008) 1–16, https://doi.org/10.1088/1367-2630/10/4/043009.
[32] M. Arienti, W. Pan, X. Li, G. Karniadakis, Many-body dissipative particle dynamics simulation of liquid/vapor and liquid/solid interactions, J. Chem. Phys. 134 (2017) 204114, https://doi.org/10.1063/1.3590376.
[33] C. Chen, C. Gao, L. Zhuang, X. Li, P. Wu, J. Dong, J. Lu, A many-body dissipative particle dynamics study of spontaneous capillary imbibition and drainage, Langmuir 26 (2010), https://doi.org/10.1021/la100105f.
[34] H. Lei, D.A. Fedosov, G.E. Karniadakis, Time-dependent and outflow boundary conditions for dissipative particle dynamics, J. Comput. Phys. 230 (2011) 3765–3779, https://doi.org/10.1016/j.jcp.2011.02.003.
[35] Z. Li, Y.H. Tang, H. Lei, B. Caswell, G.E. Karniadakis, Energy-conserving dissipative particle dynamics with temperature-dependent properties, J. Comput. Phys. 265 (2014) 113–127, https://doi.org/10.1016/j.jcp.2014.02.003.

[36] C. Chen, K. Lu, L. Zhuang, X. Li, J. Dong, J. Lu, Effective fluid front of the moving meniscus in capillary, Langmuir (2013), https://doi.org/10.1021/la304598h.

[37] S.K. Ranjith, B.S.V. Patnaik, S. Vedantam, No-slip boundary condition in finite-size dissipative particle dynamics, J. Comput. Phys. 232 (2013) 174–188, https://doi.org/10.1016/j.jcp.2012.07.046.

[38] C.C. Chang, Y.J. Sheng, H.K. Tsao, Wetting hysteresis of nanodrops on nanorough surfaces, Phys. Rev. E 94 (2016) 1–8, https://doi.org/10.1103/PhysRevE.94.042807.

[39] J. Zhao, S. Chen, N. Phan-Thien, Viscometric flow for a many-body dissipative particle dynamics (MDPD) fluid with Lees–Edwards boundary condition, Mol. Simul. 7022 (2018) 1–12, https://doi.org/10.1080/08927022.2017.1364379.

[40] N. Kadoya, N. Arai, Size dependence of static polymer droplet behavior from many-body dissipative, Phys. Rev. E 043109 (2017) 3, https://doi.org/10.1103/PhysRevE.95.043109.

[41] P.B. Paramonov, S.F. Lyuksyutov, Density-functional description of water condensation in proximity of nanoscale asperity, J. Chem. Phys. 123 (2005), https://doi.org/10.1063/1.2007632.

[42] A.A. Hemeda, R.J.A. Esteves, J.T.M. McLeskey Jr., M. Khraisheh, Molecular dynamic simulations of fibrous distillation membranes, Int. Commun. Heat Mass Transf. 98 (2018) 304–309, https://doi.org/10.1016/j.icheatmasstransfer.2018.09.012.

[43] I. Pagonabarraga, D. Frenkel, Dissipative particle dynamics for interacting systems, J. Chem. Phys. 115 (2001) 5015–5026, https://doi.org/10.1063/1.1396848.

[44] I.V. Pivkin, G.E. Karniadakis, Controlling density fluctuations in wall-bounded dissipative particle dynamics systems, Phys. Rev. Lett. 96 (2006) 1–4, https://doi.org/10.1103/PhysRevLett.96.206001.

[45] H. Dobbs, The modified Young's equation for the contact angle of a small sessile drop from an interface displacement model, Int. J. Mod. Phys. B 13 (1999) 3255–3259, https://doi.org/10.1142/S0217979299003003.

[46] A. Marmur, Wetting on hydrophobic rough surfaces: to be heterogeneous or not to be?, Langmuir 19 (2003) 8343–8348, https://doi.org/10.1021/la0344682.